Applied Catalysis A: General 473 (2014) 90–95

Contents lists available at ScienceDirect

Applied Catalysis A: General

journal homepage: www.elsevier.com/locate/apcata

Photocatalytic reduction of CO_2 in cyclohexanol on CdS–TiO_2 heterostructured photocatalyst

Guixian Song [a], Feng Xin [a,*], Jingshuai Chen [a], Xiaohong Yin [b,*]

[a] School of Chemical Engineering and Technology, Tianjin University, Tianjin 300072, China
[b] School of Chemistry and Chemical Engineering, Tianjin University of Technology, Tianjin 300384, China

ARTICLE INFO

Article history:
Received 1 September 2013
Received in revised form
26 December 2013
Accepted 29 December 2013
Available online 4 January 2014

Keywords:
Photocatalytic reduction
CO_2
Heterostructured photocatalyst
CdS–TiO_2
Nanosheets
Cyclohexanol

ABSTRACT

A nanosheet of CdS–TiO_2 with heterojunction was prepared by a two-step hydrothermal synthesis method and used as a photocatalyst for reducing CO_2 in cyclohexanol. This heterostructured composite has been characterized by X-ray diffractometer (XRD), transmission electron microscopy (TEM), X-ray photoelectron spectroscopy (XPS) and ultraviolet-visible (UV–vis) diffuse reflectance spectroscopy (DRS). The activity of the CdS–TiO_2 composite was tested in a batch slurry bed reactor. The results showed that CO_2 absorbed in cyclohexanol was reduced to cyclohexyl formate (CF) on conduction band and the absorbent cyclohexanol was oxidized to cyclohexanone (CH) on valance band of the photocatalyst. It was revealed that the highest formation rates of 20.2 μmol/(g_{cat} h) and 20.0 μmol/(g_{cat} h) for CF and CH could be obtained when TiO_2/CdS with the molar ratio of 8 was used. Overall, this work provides a novel pathway for photocatalytically reducing CO_2 and preventing the catalyst from photocorrosion.

1. Introduction

In recent years, the increasingly anthropogenic carbon emission has become a severe global environmental issue because of its serious impacts on climate change and energy source exhaustion, such as the "greenhouse effect" [1]. On the other hand, CO_2 provides carbon resource of fossil fuel in natural photosynthesis process. Therefore, seeking for renewable and recycling energies from CO_2 not only meets the increasing energy demand, but also is of environmental benign. Reduction of CO_2 to reusable hydrocarbons using solar light is one of the best mitigation strategies for both the global climate change and the energy shortage problems [2,3].

Many researchers have been devoted to mimicking the natural photosynthesis, at ambient temperature and pressure, photocatalytic conversing CO_2 to CH_4, CO, CH_3OH, HCHO, HCOOH and so on by using water as reductant and solar light as photon source [4–7]. But their evolution rates and selectivities were still unsatisfactory, because of the weak reducibility of water and the low solubility of CO_2 in water. Among the various photocatalysts used for photocatalytic reduction of CO_2, TiO_2 is considered as the most potential photocatalyst due to its various advantages including strong stability, low cost, and nontoxicity. By now, many studies reported that nanometer-scale TiO_2 catalyst, such as nanorods, nanotubes, and nanosheets exhibited promising performance as photocatalyst. Especially, for the TiO_2 nanosheets, both the high percentage of exposed (0 0 1) facet and the large surface could offer more effective surface in the photocatalytic reaction [8–10]. However, practical application has been limited by the wider band gap of 3.2 eV and low quantum efficiency. In order to increase the photocatalytic activity of TiO_2, researchers have synthesized new TiO_2-based photocatalysts, involving surface modification by ion dopants [11], photosensitizers [12], depositing noble metals [13], and semiconductor complexes [14].

Among the complexes of semiconductors, coupling TiO_2 with narrow band gap semiconductors such as CdS, which serves as a sensitizer, could improve the charge separation efficiency [15]. Moreover, coupling two different semiconductors can transfer electron from an excited one with narrow band gap into another attached one with proper choice of conduction band potentials. So the separation of photoinduced electron and hole pair is improved and the photocatalytic efficiency is raised dramatically [16]. Published papers [17–19] have proved that the formation of the interface between CdS and TiO_2 was crucial for improving the separation and restraining the recombination of photoexcited electron–hole pairs, which enhanced the photocatalytic activity.

However, CdS–TiO_2 heterostructured photocatalyst was still scarcely employed for the photocatalytic reduction of CO_2. Since CdS has a suitable band gap energy of 2.4 eV and sufficiently

* Corresponding authors at: 92 Weijing Road, Nankai District, Tianjin, China. Tel.: +86 22 27409533; fax: +86 22 27892359.
E-mail addresses: xinf@tju.edu.cn (F. Xin), yinxiaohong@tjut.edu.cn (X. Yin).

0926-860X/$ – see front matter © 2014 Elsevier B.V. All rights reserved.
http://dx.doi.org/10.1016/j.apcata.2013.12.035

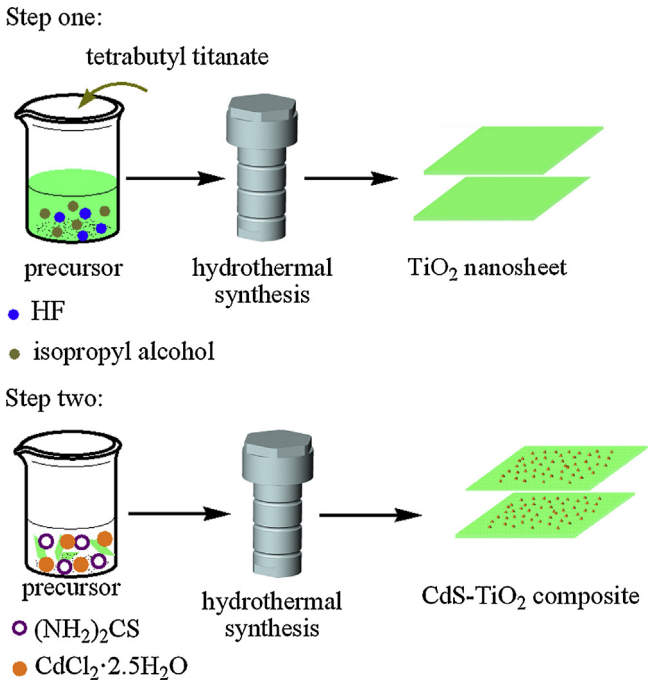

Scheme 1. Schematic plot for fabrication route of CdS–TiO_2 composite.

negative potential on conduction band of −1.0 V vs. NHE at pH = 7, we deposited CdS particles on the surface of TiO_2 nanosheets via a two-step hydrothermal method. Scheme 1 illustrated the procedure of preparing CdS–TiO_2 heterojunction photocatalyst.

In order to improve carbon dioxide solubility in the liquid phase and reducibility of the sacrificial reagent, cyclohexanol was selected as solvent and reductant because the saturated mole fraction of CO_2 in cyclohexanol is 4.43×10^{-3} [20], which is 7.5 times of that in water [21] at room temperature and normal pressure. CO_2 could be photocatalytically reduced to valuable chemicals by using cyclohexanol as reductant. Photocatalytic oxidation of cyclohexanol to CH and photocatalytic reduction of CO_2 to formic acid were occurred simultaneously, and then esterification of cyclohexanol and formic acid in bulk phase to produce CF.

CH, as one of the intermediates, is mainly used to manufacture Nylon 6, and CF is a normal solvent and synthetic perfume to be widely used in soft drinks, ice cream, frozen foods, candy, and baked food.

2. Experimental

2.1. Materials

Tetrabutyl titanate (TBOT, Ti $(OC_4H_9)_4$), hydrofluoric acid (HF, 40 wt%), isopropyl alcohol (PrOH), cadmium chloride ($CdCl_2$ $2.5H_2O$) and sulfourea ($(NH_2)_2CS$) used in synthesis of catalyst were purchased from Tianjin Guangfu Chemical Reagent Company. All reagents were analytical grade and used without any further purification. GC grade cyclohexanol ($C_6H_{12}O$) used for photocatalytic reduction of CO_2 was bought from Tianjin Xiensi Biochemical Technology Company.

2.2. Catalyst preparation

2.2.1. Preparation of TiO_2 nanosheets

Yang and co-workers [9] found synergistic functions of 2-propanol and HF on the growth of anatase TiO_2 single-crystal nanosheets. Similar to previously described work, in this paper tetrabutyl titanate was used as a titanium source instead of titanium tetrafluoride, HF and isopropyl alcohol were used as synergistic capping agent and reaction medium for preparing TiO_2 nanosheets, respectively. In a typical preparation process, 8 mL tetrabutyl titanate was added dropwise into a mixture of 1 mL hydrofluoric acid and 5 mL isopropyl alcohol with magnetic stirring for 20 min at room temperature. Then, the obtained precursor solution was transferred into a 100 mL Teflon-lined stainless steel autoclave, followed by a hydrothermal treatment at 180 °C for 24 h. After cooling down to room temperature, the collected precipitates were washed with deionized water and ethanol for three times, and dried in a vacuum oven at 80 °C for 10 h. At last, the particles were calcined at 600 °C for 2 h and pure TiO_2 nanosheets were formed.

2.2.2. Preparation of CdS–TiO_2 composite

CdS–TiO_2 composite was synthesized by hydrothermal method. Typically, 0.4 g of above TiO_2 nanosheets were added into 30 mL of deionized water and ultrasonically dispersed. Subsequently, 10 mL aqueous solution of $CdCl_2 \cdot 2.5H_2O$ and $(NH_2)_2CS$ with determined concentration were dropped into the as prepared suspension of TiO_2 nanosheets under vigorous stirring, the molar ratio of cadmium to sulfur was kept at 1:1. The final mixture was stirred for 20 min and then hydrothermally treated at 140 °C for 18 h. After centrifugal separation, the obtained precipitates were washed with ethanol and deionized water for three times, and then dried in a vacuum oven at 80 °C for 8 h.

For comparison, a series of CdS–TiO_2 photocatalysts with different molar ratios were synthesized through the same procedure by adjusting amounts of $CdCl_2 \cdot 2.5H_2O$ and $(NH_2)_2CS$, which were denoted as CdS–TiO_2-*X*, where *X* represented different molar ratios of TiO_2/CdS. Similarly, pristine CdS was also synthesized following the same procedure as mentioned above.

2.3. Catalyst characterization

The crystal structure and phase identification of the samples were analyzed with a Bruker D8 Avance XRD using Cu *K*α radiation (λ = 1.54178 nm) at 40 kV and 40 mA in the 2θ range between 20° and 80°. The morphologies of the samples were observed using Tecnai G2 F20a TEM, with accelerating voltage of 200 kV. The elemental compositions and oxidation state were analyzed by XPS (PHA-5400, SPECS, America) with Mg *K*α ADES (hν = 1253.6 eV) source at a residual gas pressure of below 10^{-8} Pa. UV–vis DRS of Shimadzu UV-2550 spectrometer were recorded in the range of 200–800 nm using $BaSO_4$ as a reference.

2.4. Photocatalytic conversion of CO_2

The photocatalytic reduction of carbon dioxide was performed in a batch slurry bed reactor with inner capacity of 50 mL in which 0.02 g of photocatalyst was dispersed in 10 mL cyclohexanol. The reactor was tightly closed during the reaction and stirred continuously by a magnetic stirrer to prevent catalyst from sedimentation. Before irradiation, ultrapure CO_2 was bubbled through the reactor for at least 30 min to purge all of dissolved oxygen and saturate absorbed CO_2. A cooling jacket with cycling water maintained the reaction at room temperature. A 250 W high pressure mercury lamp placed over the reactor to provide light irradiation. A typical run was 10 h.

After a batch, the suspension in the reactor was centrifuged to separate solid catalyst from liquid, and the supernatant solution was analyzed by an Agilent 7890A GC with a flame ionization detector (FID) and a 60 m column of HP Wax. HP1800C GC–MS was used to qualify the products and then CF and CH were found. Blank experiments were also carried out to ensure the reaction to be solely from the photocatalytic reduction of CO_2. One was light illuminated

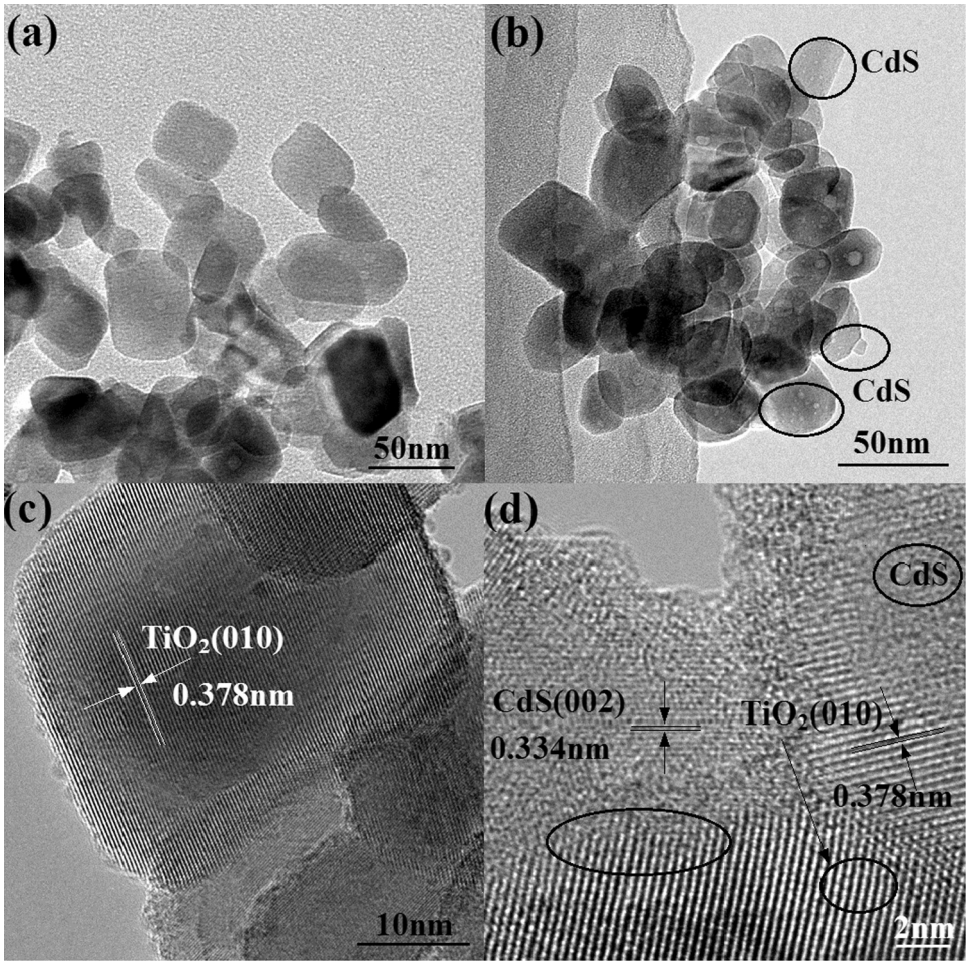

Fig. 1. TEM images of TiO_2 nanosheets (a), CdS–TiO_2-8 (b) samples and corresponding HRTEM images of TiO_2 (c) and CdS–TiO_2-8 (d) samples, respectively.

without the photocatalyst, and second was in the dark with the photocatalyst and CO_2 under the same experimental condition, third was light illuminated with the photocatalyst and bubbling N_2 rather than CO_2. No products were detected in the above three tests.

3. Results and discussions

3.1. TEM analysis

Representative TEM patterns of the photocatalysts were depicted in Fig. 1. As shown in Fig. 1(a), a number of TiO_2 nanosheets sized around 50–60 nm. The high-resolution TEM (HRTEM) image in Fig. 1(c) showed that the distance between visible lattice fringes over a large area was 0.378 nm, corresponding to the (0 1 0) facet of anatase TiO_2 [22]. Fig. 1(b) showed the CdS–TiO_2-8 composite also possesses rectangular-shape, irregular particles of CdS loaded on the surfaces of TiO_2 nanosheets. Moreover, the high resolution TEM image in Fig. 1(d) displayed clearly conjunct lattice fringes of TiO_2 and CdS. One set of the fringes spacing was about 0.334 nm, corresponding to the (0 0 2) plane of the crystallized cubic CdS [23]. Another set of the fringes spacing measured for the crystalline plane was 0.378 nm, which was ascribed to (0 1 0) plane of TiO_2. Especially, the HRTEM image in Fig. 1(d) also showed clearly that CdS particles were dispersed on the surface or bridged on the edge of the TiO_2 nanosheets. The interface between CdS and TiO_2 looked like ellipse, where nanocrystal heterojunction was formed in the composite.

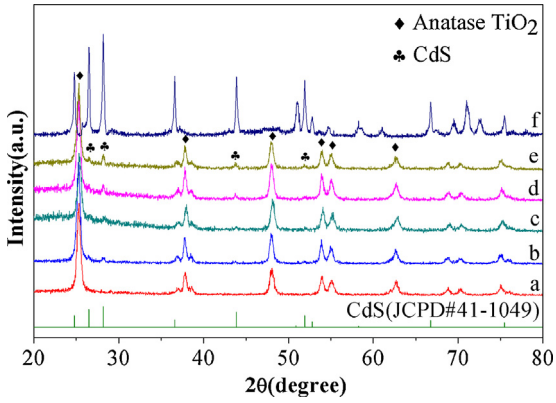

Fig. 2. XRD patterns of (a) TiO_2, (b) CdS–TiO_2-10, (c) CdS–TiO_2-9, (d) CdS–TiO_2-8, (e) CdS–TiO_2-6, (f) CdS.

3.2. XRD analysis

The crystallinity and phase of the different photocatalysts were determined by XRD. The XRD patterns of TiO_2 and CdS–TiO_2 composites in Fig. 2 showed that the characteristic peaks at 2θ of 25.3, 37.9, 48.04, 53.9, and 54.98 to be assigned to (1 0 1), (0 0 4), (2 0 0), (1 0 5), and (2 1 1) crystal planes of anatase TiO_2 (JCPDS 21-1272). In addition, all of the CdS–TiO_2 samples displayed additional diffraction peaks at 2θ of 26.48, 28.2, 43.88, and 51.94, which are attributed to (1 1 1), (0 0 2), (2 2 0), and (3 1 1) crystal planes of cubic

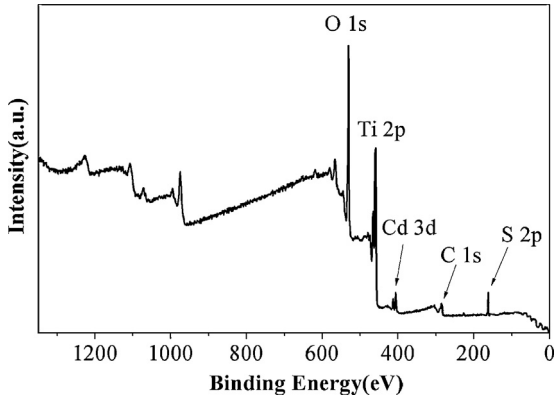

Fig. 3. XPS survey scan spectrum of the CdS–TiO_2-8 nanocomposite.

CdS crystal (JCPDS41-1049). The intensities of the peaks for the cubic CdS were increased with the increase of CdS content. The XRD patterns in Fig. 2 illustrated that the CdS presented in a separated phase rather than in the TiO_2 lattice [19].

3.3. XPS analysis

The surface compositions and elemental valences of the CdS–TiO_2-8 composite photocatalyst were determined by XPS. The fully scanned spectra in Fig. 3 showed that elements of Ti, Cd, O, S and trace of contaminated C element existed in CdS–TiO_2 heterojunction. Fig. 4 demonstrated the high-resolution XPS spectra with scanning over the area corresponding to the binding energies for Ti 2p, Cd 3d, S 2p, and O 1s. Two peaks located at 459.08 and 464.68 eV in Fig. 4(a) correspond to Ti $2p_{3/2}$ and Ti $2p_{1/2}$, respectively, indicating a normal state of Ti^{4+} in the CdS–TiO_2 heterojunction. Meanwhile, it also can be noticed from Fig. 4(b) that there is a narrow peak with a binding energy of 530.4 eV, which was attributed to the crystal lattice oxygen of Ti–O [23]. Fig. 4(c) was the high resolution XPS spectra for the Cd 3d, because of the spin–orbital splits, the Cd $3d_{5/2}$ and Cd $3d_{3/2}$ peaks also had characteristic double peaks centered at binding energies of 406.08 and 412.08 eV, respectively. These binding energies are consistent with reported values and confirm that the cadmium existed in one valence state (Cd^{2+}) in the heterojunction [24]. In Fig. 4(d), the S 2p binding energy value was 162.08 eV, which was the characteristic binding energy of CdS.

3.4. UV–vis absorption spectra analysis

The UV–vis diffuse reflectance spectra of the samples were shown in Fig. 5. The pure TiO_2 was characterized by sharp absorption edge at about 390 nm. All of CdS–TiO_2 composites synthesized with different molar ratios showed strong absorbance in the visible-light region. The band gaps (E_g) of all the samples were also estimated according to the plot of the $(\alpha h\nu)^{1/2}$ vs. photo energy ($h\nu$) [25] as shown in Fig. 6. From the extrapolated intercepts, the energy band gaps (E_g) of all the CdS–TiO_2 samples were very close to the energy band gaps of the pure TiO_2 (3.18 eV) and CdS (2.4 eV), which meant the absorption edges were not shifted for all the CdS–TiO_2 composites, Fig. 6 also indicated the spectral response of

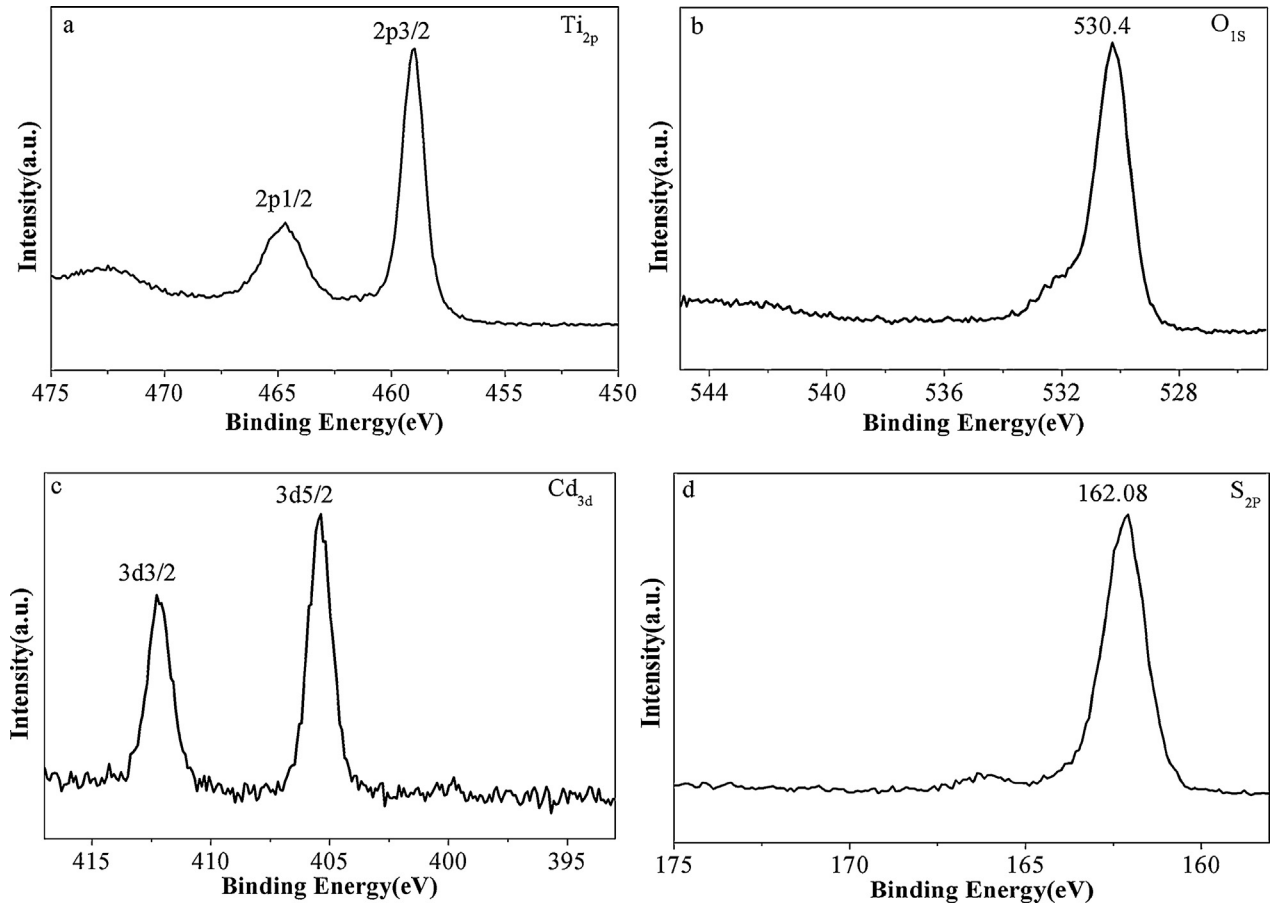

Fig. 4. XPS narrow scans for (a) Ti 2p, (b) O 1s, (c) Cd 3d, and (d) S 2p of the as-prepared CdS–TiO_2-8 nanocomposite.

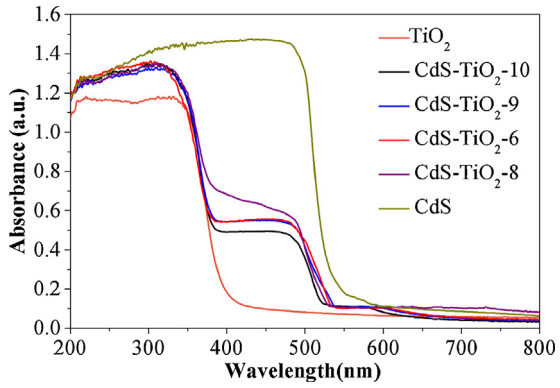

Fig. 5. UV–vis diffuse reflectance spectrum of different samples.

$CdS–TiO_2$ in visible area to be due to both TiO_2 and CdS were excited under the UV–vis spectra region. Moreover, with the increase of CdS content from 10:1 to 8:1 in samples, the absorption intensity increased correspondingly. The $CdS–TiO_2$-8 showed the most obviously absorption of visible-light. However, further increase of the TiO_2/CdS molar ratio was harmful for light absorbance because too much CdS would aggregate on the surface of TiO_2 nanosheets and thus prevent TiO_2 from absorbing light illuminate.

3.5. Photocatalytic activity

The photocatalytic activities of the samples were evaluated by photocatalytic reduction of CO_2 in cyclohexanol under UV–vis (main wave length at 360 nm) light irradiation. In the experiments, there were three products to be identified by GC/MS analysis, CF, CH and trace of cyclohexyl ether. In order to evaluate the activity of the catalysts, CF and CH were chosen as the target products. Fig. 7 showed the reaction rates of various photocatalysts in 10 h. As can be see, photocatalytic performance of TiO_2 nanosheets was slightly better than that of the Degussa-P25, which could be attributed to the larger external surface area of the nanosheets than that of nearly spheric P25 particles with the same weight. The composites of $CdS–TiO_2$ exhibited much higher activities than those of the TiO_2 nanosheets and the CdS nanoparticles owing to the strong interaction between CdS and TiO_2 and finally resulted in the capability of the photocatalytic reduction of CO_2 to be enhanced greatly. Furthermore, with the increase of CdS content in the composite from 10:1 to 8:1, the photocatalytic activities increased significantly, $CdS–TiO_2$-8 appeared an optimum photocatalytic activity at formation rates of 20.2 μmol-CF/(g_{cat} h) and 20 μmol-CH/(g_{cat} h), respectively. The production rate of CF exhibited a slightly higher than that of CH because cyclohexanol was

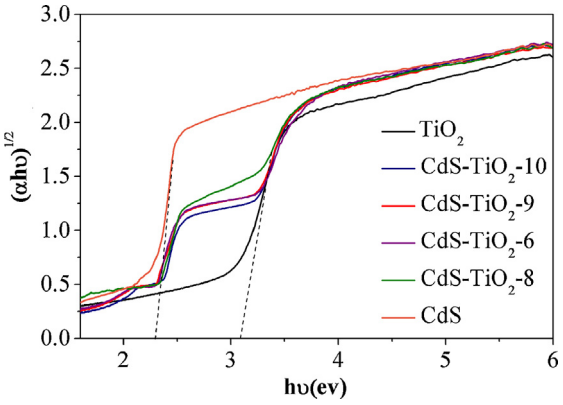

Fig. 6. Optical absorption edges of different samples.

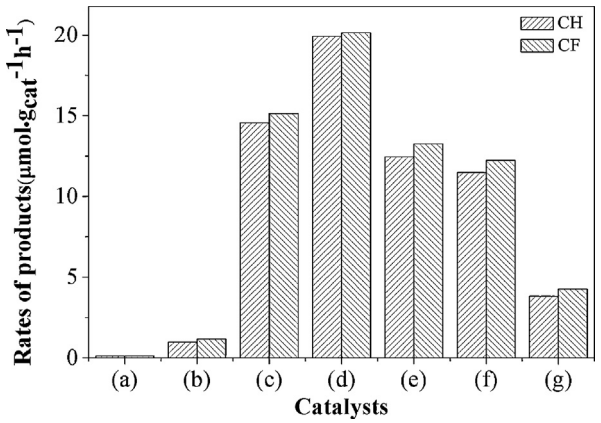

Fig. 7. The CF and CH rates in the photoreduction of CO_2 catalyzed by (a) P25; (b) TiO_2; (c) $CdS–TiO_2$-6; (d) $CdS–TiO_2$-8; (e) $CdS–TiO_2$-9; (f) $CdS–TiO_2$-10; (g) CdS.

also oxidized to cyclohexyl ether. However, further increased CdS-content would decrease the activity when the TiO_2/CdS molar ratios exceed 8, which could be attributed to too much CdS coated on the TiO_2 nanosheets. The photogenerated electrons reduced on TiO_2, consequently leading to a relatively lower activity. In our high pressure mercury lamp, the wavelength distribution was from UV to visible light. The corresponding energy density was not uniform. For completing the pathways in Scheme 2, one mole of TiO_2 excited must match one mole of excited CdS. Otherwise, the exceed electron or hole will be recombined to reduce the reaction rates.

Generally, the presence and content of CdS on TiO_2 undoubtedly played an important role in photocatalytic reduction of CO_2.

3.6. Reaction mechanism

The separation and transportation of photo-induced carriers (i.e., electrons and holes) is crucial for the photocatalytic activity. Based on our experimental results, a mechanism for photoreduction of CO_2 on the heterostructured $CdS–TiO_2$ under UV–vis light irradiation was proposed in Scheme 2. The distribution of the products in photocatalytic reduction of CO_2 was closely related to how the band energies of the photocatalyst match the redox potentials of the reaction pathways. The anodic oxidation of the cyclohexanol was at +0.85 V [26], being less than the valence band potential (E_{VB}) of TiO_2 (+2.7 V vs. NHE), which can facilitate subsequent

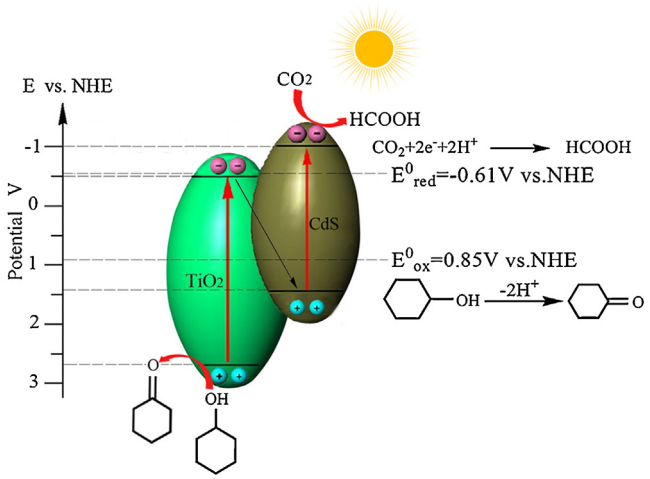

Scheme 2. Schematic view for electron–hole separations and energy band matching of $CdS–TiO_2$ heterostructure under UV–vis light irradiation.

photocatalytic oxidative reaction of cyclohexanol. The conduction band potential (E_{CB}) of CdS was −1.0 V (vs. NHE), which was more negative than that of E^0 (CO_2/HCOOH) [27]. CF was produced by the esterification reaction between formic acid and cyclohexanol [28]. Photocatalytic performance by CdS–TiO_2 composite demonstrated in this work proved that junction effect between two crystallites was also crucial for CO_2 photoeduction.

4. Conclusions

Heterojunction of CdS nanoparticles deposited on the surface of TiO_2 nanosheets were prepared by hydrothermal synthesis. TEM image revealed that CdS irregular particles were deposited on the surface of TiO_2. The obtained CdS–TiO_2 nanocomposite was proved to have remarkable performance for photocatalytic reduction of CO_2 in cyclohexanol under UV–vis light irradiation, with CF and CH as the major products. Around 20.2 μmol-CF/(g_{cat} h) and 20 μmol-CH/(g_{cat} h) were produced when using TiO_2/CdS with an optimum molar ratio of 8, which had been better enhanced photocatalytic activity than the pure TiO_2 and CdS. The mechanism for photocatalytic reduction of CO_2 in cyclohexanol to CH and CF was proposed and explained by band theory.

Acknowledgements

Gratefully thanks for the supports of the National Natural Science Foundation of China (21176192), the Tianjin natural science foundation (no. 12JCZDJC29400) and Program for Changjiang Scholars and Innovative Research Team in University (PCSIRT, no. IRT0936).

References

[1] Y. Zhou, Z. Tian, Z. Zhao, Q. Liu, J. Kou, X. Chen, J. Gao, S. Yan, Z. Zou, ACS Appl. Mater. Interfaces 3 (2011) 3594–3601.
[2] X. Chen, Y. Zhou, Q. Liu, Z. Li, J. Liu, Z. Zou, ACS Appl. Mater. Interfaces 4 (2012) 3372–3377.
[3] X. Li, H. Liu, D. Luo, J. Li, Y. Huang, H. Li, Y. Fang, Y. Xu, L. Zhu, Chem. Eng. J. 180 (2012) 151–158.
[4] P.L. Richardson, M.L.N. Perdigoto, W. Wang, R.J.G. Lopes, Appl. Catal., B 132–133 (2013) 408–415.
[5] Z. Huo, M. Hu, X. Zeng, J. Yun, F. Jin, Catal. Today 194 (2012) 25–29.
[6] R.K. Yadav, J.O. Baeg, G.H. Oh, N.J. Park, K.J. Kong, J. Kim, D.W. Hwang, S.K. Biswas, J. Am. Chem. Soc. 134 (2012) 11455–11461.
[7] K. Iizuka, T. Wato, Y. Miseki, K. Saito, A. Kudo, J. Am. Chem. Soc. 133 (2011) 20863–20868.
[8] K. Lv, Q. Xiang, J. Yu, Appl. Catal., B 104 (2011) 275–281.
[9] H.G. Yang, G. Liu, S.Z. Qiao, C.H. Sun, Y.G. Jin, S.C. Smith, J. Zou, H.M. Cheng, G.Q. Lu, J. Am. Chem. Soc. 131 (2009) 4078–4083.
[10] H.G. Yang, C.H. Sun, S.Z. Qiao, J. Zou, G. Liu, S.C. Smith, H.M. Cheng, G.Q. Lu, Nature 453 (2008) 638–641.
[11] Q. Zhang, T. Gao, J.M. Andino, Y. Li, Appl. Catal., B 123 (124) (2012) 257–264.
[12] X.Z. Li, F.B. Li, Environ. Sci. Technol. 35 (2001) 2381–2387.
[13] W.N. Wang, W.J. An, B. Ramalingam, S. Mukherjee, D.M. Niedzwiedzki, S. Gangopadhyay, P. Biswas, J. Am. Chem. Soc. 134 (2012) 11276–11281.
[14] D. Sarkar, C.K. Ghosh, S. Mukherjee, K.K. Chattopadhyay, ACS Appl. Mater. Interfaces 5 (2013) 331–337.
[15] C. Cao, C. Hu, W. Shen, S. Wang, Y. Tian, X. Wang, J. Alloys Compd. 523 (2012) 139–145.
[16] J. Mu, B. Chen, M. Zhang, Z. Guo, P. Zhang, Z. Zhang, Y. Sun, C. Shao, Y. Liu, ACS Appl. Mater. Interfaces 4 (2012) 424–430.
[17] D. He, M. Chen, F. Teng, G. Li, H. Shi, J. Wang, M. Xu, T. Lu, X. Ji, Y. Lv, Y. Zhu, Superlattices Microstruct. 51 (2012) 799–808.
[18] V.M. Daskalaki, G.L. Puma, D.I. Kondarides, P. Lianos, Environ. Sci. Technol. 44 (2010) 7200–7205.
[19] Y. Huo, X. Yang, J. Zhu, H. Li, Appl. Catal., B 106 (2011) 69–75.
[20] R. Battino, E. Wilhelm, Chem. Rev. 73 (1973) 1–9.
[21] O.K.V. Somnath, C. Roy, M. Paulose, C.A. Grimes, ACS Nano 4 (2010) 1259–1278.
[22] H. Xu, S. Ouyang, P. Li, T. Kako, J. Ye, ACS Appl. Mater. Interfaces 5 (2013) 1348–1354.
[23] S. Ding, X. Yin, X. Lu, Y. Wang, F. Huang, D. Wan, ACS Appl. Mater. Interfaces 4 (2012) 306–311.
[24] E.A. Kozlova, S.V. Cherepanova, T.P. Lyubina, E.Y. Gerasimov, V.V. Kaichev, A.V. Vorontsov, S.V. Tsybulya, A.A. Rempel, V.N. Parmon, J. Photochem. Photobiol., A 250 (2012) 103–109.
[25] Y. You, L. Wan, S. Zhang, D. Xu, Mater. Res. Bull. 45 (2010) 1850–1854.
[26] B. Srinivas, K. Lalitha, P.A.K. Reddy, G. Rajesh, V.D. Kumari, M. Subrahmanyam, B.R. De, Res. Chem. Intermed. 37 (2011) 1069–1086.
[27] M. Mikkelsen, Jørgensen, Mikkel, Krebs, C. Frederik, Energy Environ. Sci. 3 (2010) 43–81.
[28] S. Qin, F. Xin, Y. Liu, X. Yin, W. Ma, J. Colloid Interface Sci. 356 (2011) 257–261.